high v_P of cratonic lower crust and our observation of high Poisson's ratio strongly suggests a mafic composition rather than high pore pressure. With our limited data, we observe no systematic difference between Archaean and Proterozoic crust, in contrast to some previous studies[22].

We interpret the low Poisson's ratio (0.25) for Cenozoic–Mesozoic crust as indicating a predominantly felsic composition. The higher values for older crust are interpreted as reflecting a more intermediate-to-mafic composition. Specifically, Precambrian cratons have a bimodal composition distribution with a felsic-to-intermediate upper crust and a mafic lower crust. These conclusions have several possible implications for continental crustal evolution. Two main processes have been invoked in continental growth: the amalgamation of island arcs onto the edges of pre-existing continents, and pervasive intrusion and underplating of magmas derived from the upper mantle[23]. Both processes add predominantly mafic components to the crust[24,25]. The felsic composition of young orogens then implies that if magmatic addition occurs during orogenesis, either a delamination-type process must operate to remove the mafic component[24], or there is little new crust added by magmatic processes, and young orogenies mainly involve reworking of existing continental crust[26]. If the orogeny involves remobilization of an older and more mafic crust, again, some refining process such as delamination must operate to produce a predominantly felsic crust. If delamination is a common process, it raises the question of why older crust is more mafic.

There are two endmember scenarios. In a uniformitarian model, continental crust grows by amalgamation of island arc (mafic) terranes but evolves toward a more intermediate composition, first by delamination of a mafic lower crust during continental collisions. Then the remaining felsic crust is stabilized with a more mafic composition by pervasive underplating of mantle-derived magmas[27]. In this scenario young orogens, which have a felsic composition, involve crust that has not yet evolved to completion. Alternatively, the Precambrian cratons may have evolved in an entirely different manner, by a process that generated an initially more intermediate-to-mafic crust that stabilized by developing a refractory mantle root close to the time of crust formation[28]. In this scenario, processes in young orogens are fundamentally different from the processes active in the Precambrian; young orogens involve recycling and refining of existing continental crust with little crustal growth[26]. □

Received 11 August 1994; accepted 10 January 1995.

1. Christensen, N. I. & Fountain, D. M. *Geol. Soc. Am. Bull.* **86,** 227–236 (1975).
2. Holbrook, W. S., Mooney, W. D. & Christensen, N. I. in *Continental Lower Crust* (eds Fountain, D. M., Arculus, R. & Kay, R.) 1–43 (Elsevier, Amsterdam, 1992).
3. Percival, J. A., Fountain, D. M. & Salisbury, M. H. in *Continental Lower Crust* (eds Fountain, D. M., Arculus, R. & Kay, R.) 317–362 (Elsevier, Amsterdam, 1992).
4. Rudnick, R. L. in *Continental Lower Crust* (eds Fountain, D. M., Arculus, R. & Kay, R.) 269–316 (Elsevier, Amsterdam, 1992).
5. Farmer, G. L. in *Continental Lower Crust* (eds Fountain, D. M., Arculus, R. & Kay, R.) 363–390 (Elsevier, Amsterdam, 1992).
6. Kern, H. in *High-Pressure Researches in Geoscience* (ed. Schreyer, W.) 15–45 (Schweizerbart'sche, Stuttgart, 1982).
7. Owens, T. J., Zandt, G. & Taylor, S. R. *J. geophys. Res.* **89,** 7783–7795 (1984).
8. Langston, C. A. *J. geophys. Res.* **84,** 4749–4762 (1979).
9. Ammon, C. J. *Bull. seism. Soc. Am.* **81,** 2504–2510 (1991).
10. Owens, T. J. & Zandt, G. *Geophys. Res. Lett.* **12,** 705–708 (1985).
11. Zandt, G., Myers, S. C. & Wallace, T. C. *J. geophys. Res.* (in the press).
12. Clarke, T. J. & Silver, P. G. *Geophys. Res. Lett.* **20,** 241–244 (1993).
13. Hughes, S. & Luetgert, J. H. *J. geophys. Res.* **96,** 16471–16494 (1991).
14. Hughes, S. & Luetgert, J. H. *J. geophys. Res.* **97,** 17455–17479 (1992).
15. Jordan, T. H. & Frazer, L. N. *J. geophys. Res.* **80,** 1504–1517 (1975).
16. Condie, K. C. *Plate Tectonics and Crustal Evolution* (Pergamon, New York, 1989).
17. Zandt, G., Velasco, A. & Beck, S. L. *Geology* **22,** 1003–1006 (1994).
18. Taylor, S. R. & McLennan, S. M. *The Continental Crust: its Composition and Evolution* (Blackwell Scientific, Oxford, 1985).
19. Fountain, D. M. & Christensen, N. I. in *Geophysical Framework of the Continental United States* (eds Pakiser, L. C. & Mooney, W. D.) 711–742 (Geol. Soc. Am. Mem. 172, Boulder, Colorado, 1989).
20. Cassidy, J. F. & Ellis, R. M. *J. geophys. Res.* **98,** 4407–4421 (1993).
21. Christensen, N. I. in *Geophysical Framework of the Continental United States* (eds Pakiser, L. C. & Mooney, W. D.) 783–798 (Geol. Soc. Am. Mem. 172, Boulder, Colorado, 1989).
22. Durrheim, R. J. & Mooney, W. D. *Geology* **19,** 606–609 (1991).
23. Rudnick, R. *Nature* **347,** 711–712 (1990).
24. Kay, R. W., Kay, S. M. & Arculus, R. J. in *Continental Lower Crust* (eds Fountain, D. M., Arculus, R. & Kay, R.) 423–445 (Elsevier, Amsterdam, 1992).
25. Kay, R. W. & Kay, S. M. *Geology* **13,** 461–464 (1985).
26. Armstrong, R. L. *Australian J. Earth Sci.* **38,** 613–630, 1991.
27. Nelson, K. D. *Geophys. J. Int.* **105,** 25–35 (1991).
28. Hoffman, P. F. in *Allochthonous Terranes* (eds Dewey, J. F., Gass, I. G., Curry, G. B., Harris, N. B. W. & Sengor, A. M. C.) 67–76 (Cambridge Univ. Press, 1990).
29. Meissner, R. *The Continental Crust, a Geophysical Approach* (Academic, Orlando, 1986).

ACKNOWLEDGEMENTS. We thank the staff at the seismic data centers of IRIS, POSEIDON, ORFEUS, GEOSCOPE, the US National Seismic Network, the Canadian National Seismic Network, the Berkeley Digital Seismic Network, and Caltech's TERRAscope for creating and maintaining an exemplary global resource for seismic analyses. Discussions with P. Coney led to a more balanced interpretation. We thank N. I. Christensen and W. D. Mooney for reviews. This work was supported by the Institute of Geophysics and Planetary Physics at Lawrence Livermore National Laboratory.

Complex morphology of subducted lithosphere in the mantle beneath the Tonga trench

Rob van der Hilst

Research School of Earth Sciences,
The Australian National University, Canberra, ACT 0200, Australia

AT the Tonga trench, old Pacific sea floor subducts at a rapid rate below the Indo-Australia plate, generating most of the world's deep earthquakes (focal depth >300 km)[1,2] and producing a deep slab of former oceanic lithosphere. The seismogenic part of the slab has been mapped in detail[3,4], but its fate has remained enigmatic. Here I present evidence from seismic tomography that the Pacific plate descends deep into the Earth's mantle along a trajectory that is more complex than previously thought. In the north, the slab deflects in the transition zone (between about 400 and 700 km depth) before continuing into the lower mantle (below 700 km). Further south, penetration into the lower mantle occurs without a kink. The slab morphology can be explained in terms of the recent tectonic evolution of the subduction system, and reconciles pre-existing evidence from this region for both local horizontal flow in the transition zone[2–8] and slab penetration into the lower mantle[9–12].

In the southwest Pacific (Fig. 1*a*) the large age (>120 Myr) of oceanic lithosphere and the high rate of subduction (>10 cm yr^{-1})[13] combine to produce a deep, negatively buoyant slab of former oceanic lithosphere. This slab was the subject of pioneering work on deep seismicity that further substantiated the concept of plate tectonics[2,5,6]. Analyses of travel times of seismic waves revealed fast P-wave propagation below the deepest earthquakes, suggesting the continuation of the slab into the Earth's lower mantle[9–12]. On the other hand, locations and focal mechanisms of deep earthquakes indicate internal deformation and horizontal flow in the transition zone[2,9,14] which has been interpreted as evidence against the continuation of the slab below 700 km depth, or for the detachment of the slab[7,14,15].

In a recent tomographic study R.v.d.H. and E. R. Engdahl (manuscript in preparation) used nearly 10^6 travel times of first and later-arriving compressional waves to map mantle structure to a depth of 1,600 km below the Fiji–Tonga region. Earthquake locations and phase data resulted from nonlinear hypocentre relocation and phase re-identification using arrival times from the International Seismological Centre[16,17]. Results of this investigation confirm some inferences from an earlier study[11], but the new images are of improved quality owing to better (and more) phase data and hypocentres, denser sampling due to inclusion of later-arriving phases, and the use of the iasp91 reference model[16,18]. Moreover, they are given a different interpretation. Here I focus on the relationship between large-scale slab structure and lateral displacement of the Tonga subduction system. Mantle structure further north is complex, owing to the subduction of the New Hebrides basin beneath the clockwise-migrating

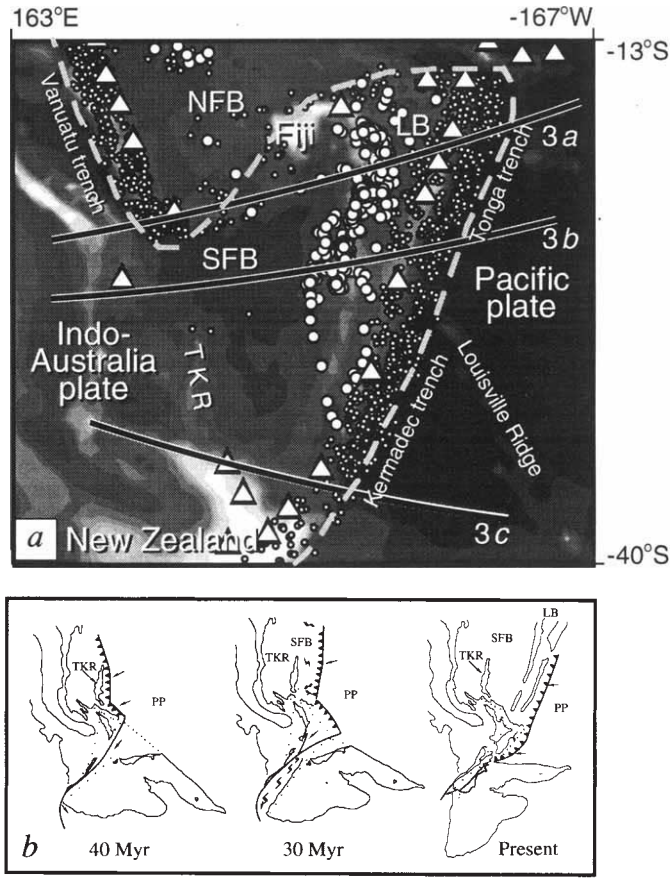

FIG. 1 *a*, The southwest Pacific study region (Cartesian map projection). Shading indicates water depth (dark, deep; light, shallow). Dashed line, boundary between the Pacific and Indo-Australia plates; white dots, epicentres of earthquakes (after E. R. Engdahl, R.v.d.H. and R. Buland, manuscript in preparation) with Richter scale magnitude >5.2 (small dots, focal depth <70 km; large dots, depth >300 km). Triangles, sites of active (Holocene–present) arc volcanism. Lines labelled '3*a*', '3*b*' and '3*c*' give the position of the mantle cross-sections displayed in Fig. 3. *b*, Approximate position of the Tonga–Kermadec trench at intermediate stages (40 Myr ago, 30 Myr ago, and present day) during the post-Eocene clockwise migration of the Tonga trench (after Walcott[38]). This rotation is superimposed on possible northward motion of the shallow part of the subduction system relative to the deeper mantle[8,9]. Abbreviations used: SFB, South Fiji basin; NFB, North Fiji basin; LB, Lau basin; TKR, Three Kings rise; PP, Pacific plate.

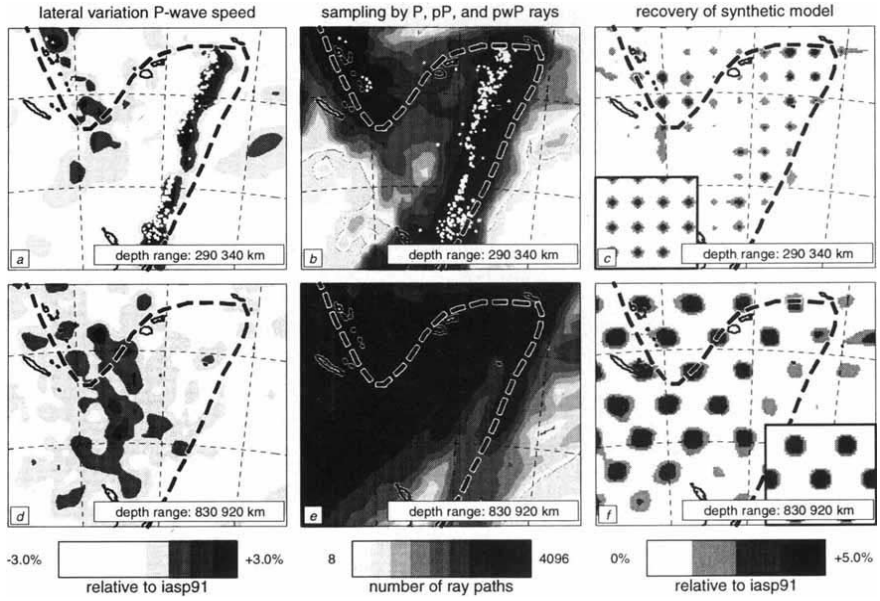

FIG. 2 Results of tomographic inversions R.v.d.H. and E. R. Engdahl, manuscript in preparation). *a*, Lateral variation in P-wave velocity below the study region at ~300 km depth. Regions of fast wave propagation are depicted by shading in order to emphasize slab structure. Seismicity is depicted by white dots. At this depth, P waves in the slab propagate up to 4% faster than average. *b*, Spatial distribution of ray paths used in the inversion. *c*, Recovery of a synthetic model consisting of velocity anomalies with a horizontal dimension of $0.9° \times 0.9°$ ($\sim 95 \times 95$ km^2 at this depth). Using the ray distribution as in the actual data inversion, synthetic data were generated from this model and inverted with the objective of recovering the input model[42]. The position of the synthetic anomalies is recovered near the slab but the amplitude of the input signal is not well resolved. Resolution degrades with increasing distance away from the slab owing to irregular sampling. Artificial errors were not added to the synthetic data. The regular pattern of the input model is depicted in the inset; the recovery of this pattern is displayed in the main part of the figure. *d*, Velocity anomaly (up to 2% fast) in the lower mantle at a depth of ~900 km. *e*, Sampling at 900 km depth. *f*, Synthetic anomalies used to test resolution of lower-mantle structure have a horizontal dimension of $1.8° \times 1.8°$ ($\sim 170 \times 170$ km^2 at 900 km depth) (inset), and are adequately recovered in a large region around the structural feature depicted in *d*. Spatial resolution degrades to the east of the slab. The variation in wave speed is relative to the iaspg model; the sampling is given as the number of ray paths, propagating through a particular part of the model.

METHODS. The images *a*, *c*, *d* and *f* resulted from a damped linearized inversion[16,42] of travel-time data of first-arriving P waves, that is compressional seismic waves propagating directly from source to receiver, and the later-arriving depth phases (pP and pwP), which travel initially upwards from the source and reflect at the surface of the Earth (water-sediment/water–atmosphere interface for pP/pwP). The data were obtained from a nonlinear relocation and phase re-identification procedure using arrival times published by the International Seismological Centre (ISC) and ISC hypocentres as initial values (E. R. Engdahl, R.v.d.H. and R. Buland, manuscript in preparation). The combination of P, pP, and pwP data improves the sampling of structure and the constraints on earthquake focal depth, and reduces the trade-off between hypocentre mislocation and aspherical variations in seismic velocity[16,17].

Vanuatu trench. Further south, westward subduction beneath the North Island of New Zealand began only recently (<10 Myr ago), is probably unrelated to the deep slab discussed here, and the evolution of the southern Kermadec arc is still controversial (R. Walcott, personal communication).

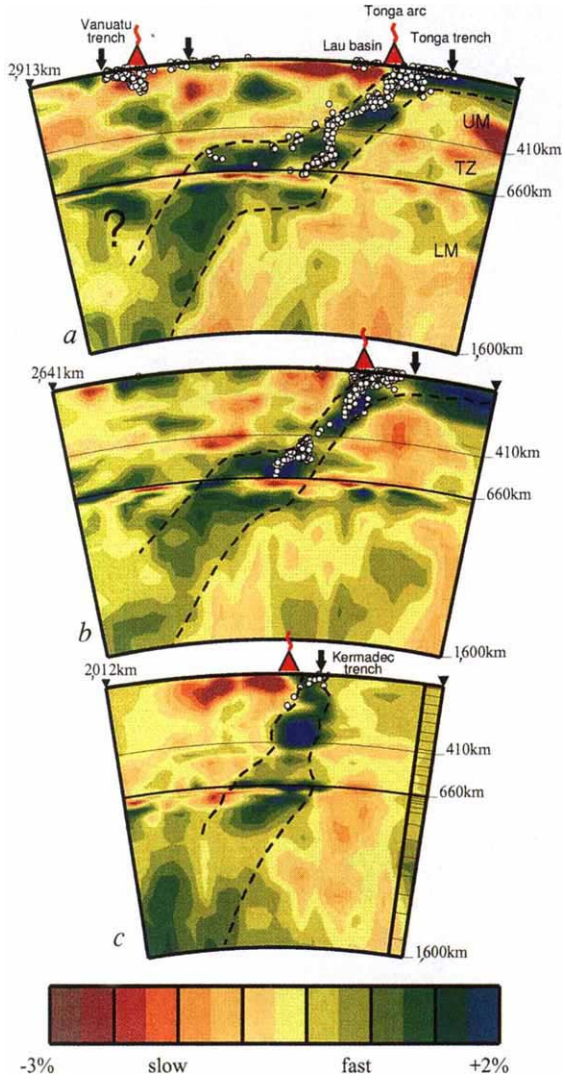

FIG. 3 Tomographic images of aspherical variations in P-wave velocity in the mantle below northern Tonga (*a*), central Tonga (*b*) and Kermadec (*c*). See Fig. 1 for location of the cross-sections. Green-blue colours, mantle regions where P-wave velocity is faster than the iasp91 reference model[18] at the same depth; white dots, earthquake hypocentres projected from a distance of up to 50 km on each side of the plane of cross-section. Black arrows (red triangles) mark the intersection of the line of cross-section with the plate boundary (volcanic arc). A prominent feature, schematically outlined by dashed lines, is the zone of fast seismic velocity dipping into the mantle at the trench and delineated by seismicity in the upper mantle (UM) and transition zone (TZ), and aseismic in the lower mantle (LM). Slow P-wave propagation is evident below volcanic arcs and regions of recent or active back-arc spreading such as the Lau basin, and also adjacent to the slab in the deeper mantle. This was also observed by Zhou[11]. At large depths some of this signal is an artefact from the mapping of the fast slab (Fig. 4).
METHODS. In vertical direction, the dimension of the blocks used to parametrize the mantle volume under study varies from 35 km near the Earth's surface to 200 km in the lower mantle. One column of the block model is superimposed on the image at the right-hand side of Fig. 3c. Between 590 and 730 km depth, thin layers (~15 km) are used to detect possible rapid variations in P-wave velocity near the "660 km" discontinuity and to confine to a narrow depth range artificial structure due to inadequate representation of the discontinuity in the reference model.

Seismic tomography images 'cold' slabs of subducted lithosphere as regions of fast wave propagation. Figure 2*a* shows a seismic velocity anomaly associated with the subducted Pacific plate in the upper mantle that is virtually parallel to the trench and delineated by seismicity. Although the sampling of mantle structure is irregular, it is dense near the feature interpreted as subducted lithosphere (Fig. 2*b*). Consistent with results of global imaging[19], Fig. 2*d* reveals a seismic velocity anomaly in the lower mantle with an orientation that differs significantly from the strike of the present-day trench. Its position is not controlled in a trivial way by the distribution of the ray paths (Fig. 2*e*). The angle, measured in horizontal plane, between the orientation of the slab-like structures at depth of 300 and 900 km is ~35°.

As expected from the images in map-view, vertical sections across the trench reveal considerable variation in slab structure along the strike of the arc (Fig. 3). In the north, the Pacific plate descends into the upper mantle at an angle of ~50° and becomes almost horizontal in the transition zone and uppermost lower mantle (Fig. 3*a*). This deflection is consistent with inferences from seismicity[2–9,14]. However, the slab is not trapped in the transition zone but sinks deeper into the lower mantle several hundred kilometres further west. The deep earthquakes below the Fiji basin, previously interpreted as evidence for detached parts of subducted lithosphere[6,14,15], are located in the continuous slab. Vertically below the inclined seismic zone, the slab is imaged to a depth of ~800 km. This is in agreement with evidence from residual sphere analyses of travel times[9,10], which may have detected only part of the complex slab structure. Towards the south, both the seismic zone[3,4] and the slab become steeper, and the kink of the slab across the transition zone disappears (Fig. 3*b*, *c*).

In the upper mantle and transition zone, the lateral variation of slab morphology is well resolved (Fig. 2*c*) and is consistent with the geometry of seismic zones[3,4] (Fig. 2*a*). To assess image reliability for depths beyond seismicity additional testing is required. Inversion of subsets of the data produces similar solutions demonstrating that the imaging is robust. In addition, the recovery of a synthetic velocity model indicates that the structural feature in the lower mantle (Fig. 2*d*) is well resolved (Fig. 2*f*). However, a slight degradation of the spatial resolution to the east leaves the possibility that the deep slab is actually broader than imaged in Fig. 3*a*. Its steep, eastern part can be overlooked if it is not sampled effectively by the ray paths used. The potential recovery of a broad slab is tested explicitly by inverting travel-time data computed from a model slab inspired by work of Fischer and colleagues[9,10] (Fig. 4*a*). The adequate recovery of the model (Fig. 4*b*) demonstrates that the lower-mantle slab cannot be significantly thicker than depicted in Fig. 3*a* because this would have been detected in the actual inversion. Similarly, inversion of data computed from a synthetic upper-mantle slab model (Fig. 4*c*) demonstrates that the lower-mantle anomaly does not result from the smearing of structure at shallower depths (Fig. 4*d*). The low velocities just below 410 and 660 km depth (Fig. 3) are reference-model artefacts[16] indicating that, locally, the increase in P-wave velocity across the discontinuities is either smaller or occurs at a larger depth than in the global iasp91 model. Low velocities near the slab between 660 and 710 km depth (Fig. 3) concur with the inference from P-to-S wave conversion that the endothermic, isochemical phase change from spinel to post-spinel structure that coincides with the "660 km" discontinuity may be depressed by up to 50 km owing to the presence of the cold slab[20].

To understand slab morphology in terms of mantle dynamics, one should realize that the shape of the slab is a snapshot of a time-dependent process influenced by relative plate motion[21–23]. Lateral displacement of a convergent plate boundary relative to the deeper mantle can produce the observed kink in the subducting slab (Fig. 3) if slab descent is slowed down on approaching the lower mantle because of an increase in viscosity[21,24,25] and/or effects of isochemical phase changes on buoyancy[25–27]. If trench

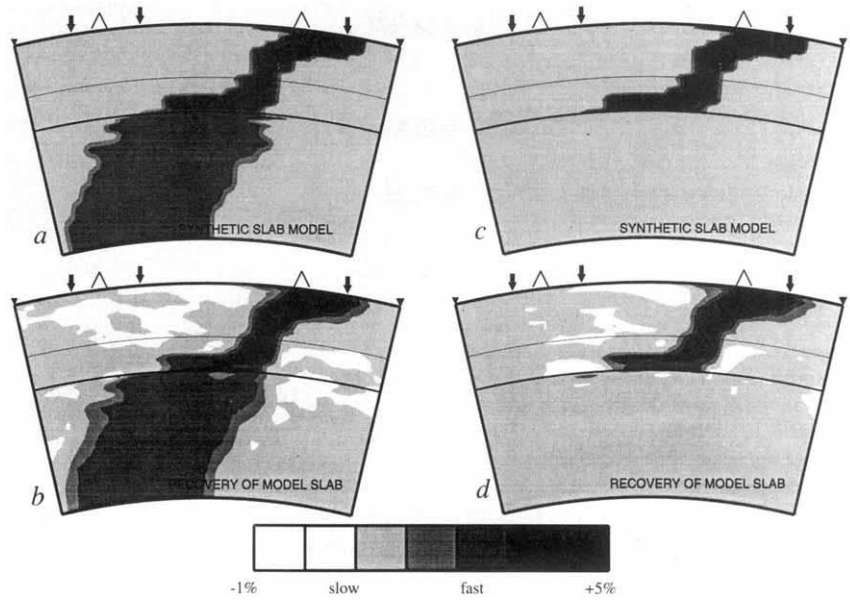

FIG. 4 Results of tests to investigate whether the deep slab can actually be broader than imaged (*a*, *b*), and whether the lower-mantle anomaly in Fig. 3*a* can result from the smearing of shallower structure (*c*, *d*). *a*, Model slab synthesized from the three-dimensional slab structure shown in Figs 2 and 3. In the upper-mantle and transition zone the slab is similar to that of Fig. 3*a*, but is artificially enlarged below 800 km depth. In the model slab, P-wave velocity is 4% faster-than-average for depths <300 km, 3% for 300–660 km, and 2% below 660 km; velocity perturbations are set to zero outside the slab. Synthetic travel-time data are computed from this model using the same ray distribution as in the actual data inversion. *b*, Recovery of the model slab. Both the shape of the model slab and the amplitude of the velocity anomalies are adequately recovered on inversion of the synthetic data. The assignment of only positive velocity anomalies to the model slab (*a*) produces a biased distribution of synthetic data. This bias is (partly) removed on least-squares inversion of the data, which produces slower-than-average wave propagation in some regions of the model space. *c*, Model slab with perturbations set to zero for depths greater than 660 km. *d*, Recovery of the model slab, showing that the shape is well recovered, although with some loss of amplitude. Note that slab structure in the upper mantle and transition zone is not mapped into lower-mantle anomalies.

migration is fast compared to the sinking velocity, the slab is (temporarily) laid down atop the more viscous lower layer before it flows to greater depth[28]. In contrast, the slab buckles without deflection if trench migration is slow compared to slab descent[21,24,29]. I now argue that the former situation may apply to northern Tonga (Fig. 3*a*) and the latter to Kermadec (Fig. 3*c*).

Subduction processes controlled the Late Palaeozoic tectonic development of east Australia[30,31], but the Pacific/Indo-Australia plate boundary has been migrating away from the continent since the Cretaceous breakup of eastern Gondwanaland. This migration has been accompanied by the progressive eastward fragmentation of arc systems and by episodes of seafloor spreading in marginal basins (Tasman sea, ~65 Myr ago; Fiji basin, 34–25 Myr; Lau basin, 5 Myr–present)[30 37]. A change in Pacific-plate motion 40–45 Myr ago probably triggered the current episode of subduction below the Indo-Australia plate[37] along the Three Kings rise, an extinct arc[35,36,38]. Subsequent changes in relative plate motion[37] caused a clockwise rotation of the Tonga–Kermadec trench, back-arc spreading in the South Fiji[35,38] and Lau basins[32,35,39–41] (Fig. 1*b*), and the initiation of westward subduction beneath New Zealand[38]. This rotation is superimposed on a possible northward motion of the plate boundary[8,9] and is estimated from tectonic reconstructions at ~20° in the past 5 Myr and possibly twice as much since the Eocene epoch (Fig. 1*b*)[38–41]. The rate of trench migration decreases from north (Fiji–Tonga) to south (Kermadec). The rotation angle is in excellent agreement with the change of the orientation of the slab with depth inferred from the tomograms (Fig. 2*a*, *d*).

Plate reconstructions and fluid-dynamical experiments provide powerful tools for the interpretation of slab morphology as revealed by seismic inversions, but causal relationships between slab deflection, trench migration and back-arc spreading are not yet completely understood. Quantitative modelling of this geodynamical system[25,27], along with continued seismological investigation, will improve our understanding of convective flow in the Earth's interior and its relationship to surface tectonics. □

Received 29 September 1994; accepted 16 January 1995.

1. Frohlich, C. *A. Rev. Earth planet. Sci.* **17,** 227–254 (1989).
2. Sykes, L. R. *J. geophys. Res.* **71,** 2981–3006 (1966).
3. Billington, S. thesis, Cornell Univ. (1980).
4. Chiu, J.-M., Isacks, B. L. & Cardwell, R. K. *Geophys. J. Int.* **106,** 99–112 (1991).
5. Oliver, J. & Isacks, B. L. *J. geophys. Res.* **72,** 4259–4275 (1967).
6. Isacks, B. L., Oliver, J. & Sykes, L. R. *J. geophys Res.* **73,** 5855–5899 (1968).
7. Baranzangi, M., Isacks, B. L., Oliver J., Dubois, J. & Pascal, G. *Nature* **242,** 98–101 (1973).
8. Giardini, D. & Woodhouse, J. H. *Nature* **307,** 505–509 (1984); *Nature* **319,** 551–555 (1986).
9. Fischer, K. M., Creager K. C. & Jordan, T. H. *J. geophys. Res.* **96,** 14403–14427 (1991).
10. Fischer, K. M. & Jordan, T. H. *J. geophys. Res.* **96,** 14429–14444 (1991).
11. Zhou, H.-W. *Phys. Earth planet. Int.* **61,** 199–229 (1990).
12. Frohlich, C. & Barazangi, M. *Phys. Earth planet. Int.* **21,** 1–14 (1980).
13. Jarrard, R. D. *Rev. Geophys.* **24,** 218–284 (1986).
14. Richter, F. M. *J. geophys. Res.* **84,** 6783–6795 (1979).
15. Hamburger, M. W. & Isacks, B. L. *J. geophys. Res.* **92,** 13841–13854 (1987).
16. Van der Hilst, R. D., Engdahl, E. R., Spakman, W. & Nolet, G. *Nature* **353,** 37–43 (1991).
17. Van der Hilst, R. D. & Engdahl, E. R. *Phys. Earth planet. Inter.* **75,** 39–53 (1992).
18. Kennett, B. L. N. & Engdahl, E. R. *Geophys. J. Int.* **105,** 848–854 (1991).
19. Vasco, D. W., Johnson, L. R., Pulliam, R. J. & Earle, P. S. *J. geophys. Res.* **99,** 13727–13755 (1994).
20. Richards, M. A. & Wicks, C. W. *Geophys. J. Int.* **101,** 1–35 (1990).
21. Gurnis, M. & Hager, B. H. *Nature* **335,** 317–321 (1988).
22. Van der Hilst, R. D. & Seno, T. *Earth. planet. Sci. Lett.* **120,** 395–407 (1993).
23. Garfunkel, Z., Anderson, C. A. & Schubert, G. *J. geophys. Res.* **91,** 7205–7224 (1986).
24. Kincaid, C. & Olson, P. *J. geophys. Res.* **92,** 13832–13840 (1987).
25. Davies, G. F. *Earth planet. Sci. Lett.* (submitted).
26. Ringwood, A. E. & Irifune, T. *Nature* **331,** 131–136 (1988).
27. Zhong, S. & Gurnis, M. *Science* (in the press).
28. Griffiths, R. W., Hackney, R. & Van der Hilst, R. D. *Earth planet. Sci. Lett.* (submitted).
29. Griffiths, R. W. & Turner, J. S. *Earth planet. Sci. Lett.* **90,** 467–477 (1988).
30. Collins, W. J. & Vernon, R. H. *Tectonophysics* **235,** 249–275 (1994).
31. Caritat, P. de & Braun, J. *J. Geodynamics* **16,** 241–281 (1992).
32. Karig, D. E. *J. geophys. Res.* **79,** 239–254 (1970).
33. Weissel, J. K., Hayes, D. E. & Herron, E. M. *Mar. Geol.* **25,** 231–277 (1977).
34. Crook, K. A. W. & Belbin, L. *J. geol. Soc. Aust.* **25,** 23–40 (1978).
35. Malahoff, A., Feden, R. H. & Fleming, H. S. *J. geophys. Res.* **87,** 4109–4125 (1982).
36. Kamp, P. J. J. *Tectonophysics* **121,** 225–251 (1986).
37. Molnar, P., Atwater, T., Mammerickx, J. & Martin, S. M. *Geophys. J. R. ast. Soc.* **40,** 383–420 (1975).
38. Walcott, R. I. *Phil. Trans. R. Soc.* A**321,** 163–181 (1987).
39. Sclater, J., Hawkins, J., Mammerickx, J. & Chase, C. *Geol. Soc. Am. Bull.* **83,** 505–518 (1972).
40. Hamburger, M. W. & Isacks, B. L. *Nature* **332,** 599–604 (1988).
41. Parson, L. M. *et al. Geology* **18,** 470–473 (1990).
42. Spakman, W. & Nolet, G. in *Mathematical Geophysics* (eds Vlaar, N. J., Nolet, G., Wortel, M. J. R. & Cloetingh, S. A. P. L.) 155–188 (Reidel, Dordrecht, 1988).

ACKNOWLEDGEMENTS. I thank J. Braun, G. Davies, R. Griffiths, S. Mazzotti, G. Nolet and R.Walcott for discussions, and M. Gurnis and B. Kennett for reviews. In collaboration with E. R. Engdahl and R. Buland, phase data and hypocentre locations were processed before tomographic inversion and I thank them for supplying data after each incremental improvement of processing.